

The presence of an additional electron in NB^- may double or triple the internal barrier and this would lead³⁰ to a loss of 1 to 2 eu in this rotation. Additional stiffening may occur in the C-N, N-O, and ring-bending vibrations of NB^- . These combined effects may be responsible for the observed negative ΔS°_7 of the nitrobenzenes.

The quinones show also negative entropy changes on electron attachment. Of the 30 vibrations of benzoquinone, there are some five CO bending modes³¹ ranging from 240 to 500 cm^{-1} . A stiffening of these modes in the presence of the electron in the benzoquinone negative ion can be expected. This could lead to a loss of a few eu.

Nitrobenzene and benzoquinone and their negative ions are well within the range of modern MO calculations. Such calculations would be of interest regarding structural changes between the neutral molecule and the corresponding negative ion.

The entropy changes on electron capture for SF_6 , C_7F_{14} , and C_6F_6 substituted perfluorophenyl compounds, see Figure 5, are discussed elsewhere.^{2,4}

(31) Becker, E. D.; Charney, E.; Anno, T. *J. Chem. Phys.* 1965, 42, 942.

van't Hoff plots were not made for all compounds whose entropy changes are shown in Table IV. Since the entropy changes, see Figure 5, are similar for similar compounds, some ΔS°_7 values were estimated. The assumptions used for these estimates are given in Table IV.

Acknowledgment. This work was supported by the Canadian Natural Sciences and Engineering Research Council.

Registry No. SO_2 , 7446-09-5; NO_2 , 10102-44-0; SF_6 , 2551-62-4; C_7F_{14} , 355-59-9; CS_2 , 75-15-0; CH_3NO_2 , 75-52-5; $\text{F}_5\text{C}_6\text{CN}$, 773-82-0; SO_2^- , 12143-17-8; 4-CINB, 100-00-5; NB, 98-95-3; Az, 275-51-4; NpQ, 130-15-4; 4-CNNB, 619-72-7; 2- CH_3NB , 88-72-2; 2,3-di CH_3NB , 83-41-0; 3,5-di NO_2NB , 99-35-4; 4- NO_2NB , 100-25-4; 3-FNB, 402-67-5; MaAn, 108-31-6; 3- CF_3NB , 98-46-4; 2,3-di ClINpQ , 117-80-6; Cl_4BQ , 118-75-2; F_4BQ , 527-21-9; 2,6- Cl_2BQ , 697-91-6; BQ, 106-51-4; 2- CH_3BQ , 553-97-9; 1,4-(CN) $_2\text{F}_4\text{C}_6$, 1835-49-0; 3,5-(CF_3) $_2\text{NB}$, 328-75-6; 3- NO_2NB , 99-65-0; 2- NO_2NB , 528-29-0; 2-CNNB, 612-24-8; 3-CNNB, 619-24-9; 3-BrNB, 585-79-5; 4-BrNB, 586-78-7; 3-CINB, 121-73-3; PhAn, 85-44-9; 2,4- F_2NB , 446-35-5; 2-BrNB, 577-19-5; F_3NB , 880-78-4; 2-CINB, 88-73-3; 4-FNB, 350-46-9; 2-FNB, 1493-27-2; 3- OCH_3NB , 555-03-3; 3- CH_3NB , 99-08-1; 4- CH_3NB , 99-99-0; 4- OCH_3NB , 100-17-4; 2,4,6-(CH_3) $_3\text{NB}$, 603-71-4; 4-FBPh, 345-83-5; BPh, 119-61-9; 3- NO_2 -5CNNB, 4110-35-4; 2,3-butanedione, 431-03-8.

CHEMICAL KINETICS

Spectrokinetic Studies of Ethyl and Ethylperoxy Radicals

Jette Munk, Palle Pagsberg,* Emil Ratajczak,[†] and Alfred Sillesen

Department of Chemistry, Risø National Laboratory, DK 4000 Roskilde, Denmark

(Received: January 2, 1985; In Final Form: January 2, 1986)

Hydrogen atoms were produced by pulse radiolysis of H_2 at 1 atm and $T = 298$ K. The yield of H atoms was determined by monitoring the UV absorption of HO_2 produced in the presence of oxygen via the reaction $\text{H} + \text{O}_2 (+\text{M}) \rightarrow \text{HO}_2 (+\text{M})$. In the presence of small amounts of C_2H_4 we observed the formation of ethyl radicals via $\text{H} + \text{C}_2\text{H}_4 (+\text{M}) \rightarrow \text{C}_2\text{H}_5 (+\text{M})$ (6) as well as the subsequent decay via $2\text{C}_2\text{H}_5 \rightarrow \text{C}_4\text{H}_{10}$, $\text{C}_2\text{H}_4 + \text{C}_2\text{H}_6$ (8). The spectrum of C_2H_5 is composed of two absorption bands with maxima at 205 and 245 nm. The 205-nm band exhibits a characteristic fine structure with a maximum extinction coefficient of $2010 \pm 300 \text{ M}^{-1} \text{ cm}^{-1}$. The weaker 245-nm band appears to be a broad continuum with an extinction coefficient of $870 \pm 130 \text{ M}^{-1} \text{ cm}^{-1}$. By computer-aided analysis of the kinetic features we have obtained values of $k_6 = (5.5 \pm 0.5) \times 10^8 \text{ M}^{-1} \text{ s}^{-1}$ and $2k_8 = (2.3 \pm 0.3) \times 10^{10} \text{ M}^{-1} \text{ s}^{-1}$. In the presence of both C_2H_4 and O_2 we observed the formation of ethylperoxy radicals, $\text{C}_2\text{H}_5 + \text{O}_2 (+\text{M}) \rightarrow \text{C}_2\text{H}_5\text{O}_2 (+\text{M})$ (10a), followed by a slow second-order decay, $2\text{C}_2\text{H}_5\text{O}_2 \rightarrow \text{products}$ (13). The spectrum of $\text{C}_2\text{H}_5\text{O}_2$ is a broad continuum with a maximum at 230 nm and $\epsilon = 1410 \pm 200 \text{ M}^{-1} \text{ cm}^{-1}$. From the observed rate of formation we obtained $k_{10a} = (3.2 \pm 0.1) \times 10^9 \text{ M}^{-1} \text{ s}^{-1}$ at $p(\text{M}) = p(\text{H}_2) = 1$ atm. From the observed second-order decay we have determined $2k_{13} = (6.3 \pm 0.3) \times 10^7 \text{ M}^{-1} \text{ s}^{-1}$. The rate of reaction 10a was studied in the range of 298–400 K, and the results may be presented in terms of an Arrhenius expression with an apparent negative activation energy, $\log k_{10a}/\text{M}^{-1} \text{ s}^{-1} = (8.90 \pm 0.04) + (840 \pm 70) \text{ cal mol}^{-1}/2.303RT$.

Introduction

Progress toward a detailed understanding of hydrocarbon oxidation has been achieved through analysis of product yields and by studies of the rate parameters of individual elementary reactions.¹⁻⁵ In the case of ethane an important step in the low-temperature oxidation is the formation of ethylperoxy radicals, $\text{C}_2\text{H}_5 + \text{O}_2 (+\text{M}) \rightarrow \text{C}_2\text{H}_5\text{O}_2 (+\text{M})$, while at higher temperatures the disproportionation reaction $\text{C}_2\text{H}_5 + \text{O}_2 \rightarrow \text{C}_2\text{H}_4 + \text{HO}_2$ becomes increasingly important. The aim of the present investigation was to study the formation and decay kinetics of ethyl and

ethylperoxy radicals by monitoring the transient absorption signals at suitable wavelengths chosen on the basis of the relative magnitude of the absorption coefficients of the two species. UV spectra of the radicals were recorded under experimental conditions where the radical yields could be determined quantitatively to obtain reliable values of the absorption coefficients. These values were

(1) G. J. Minkoff and C. F. H. Tipper, *Chemistry of Combustion Reactions*, Butterworths, London, 1962.

(2) R. T. Pollard in *Comprehensive Chemical Kinetics*, Vol. 17, C. H. Bamford and C. F. H. Tipper, Eds., Elsevier, New York, 1977, pp 249–367.

(3) G. McKay, *Prog. Energy Combust. Sci.*, 3, 105 (1977).

(4) R. R. Baldwin, J. P. Bennet, and R. W. Walker, *Symp. (Int.) Combust.*, [Proc.], 16th, 1976, 819 (1977).

(5) S. W. Benson, *Prog. Energy Combust. Sci.*, 7, 125 (1981).

[†] Department of Physical Chemistry, Medical Academy, 50-140 Wrocław, Poland.

used to convert transient absorption signals into radical concentration vs. time profiles which are required in order to determine absolute rate coefficients of radical-radical reactions. In the course of our studies we discovered some characteristic features which have not been observed in previous studies of the UV spectrum of C_2H_5 .⁶⁻⁹ Regarding the spectrum of $C_2H_5O_2$, our results are in good agreement with other recent studies.^{10,11}

Experimental Section

Apparatus and Procedures. Our experimental setup for pulse radiolysis combined with transient absorption spectrophotometry has been described previously.^{12,13} Briefly, free radicals are produced by irradiation of a gas mixture with a 30-ns pulse of 2-MeV electrons from a Febetron 705 B field emission accelerator. A pulsed 150-W Xe lamp stabilized by optical feedback provides a high UV output to ensure a good signal-to-noise ratio of transient absorption signals in the region of 200–500 nm. Via an optical system composed of Suprasil lenses, the analyzing light enters the sample cell where a set of internal aluminized spherical mirrors provide optical path lengths of 40, 80, or 120 cm by multiple reflections. The spectral features are analyzed by a 1-m grating spectrograph applying a 1200 lines/mm grating which gives a reciprocal dispersion of 8 Å/mm. The light intensity is monitored with a fast photomultiplier equipped with an S-20 cathode behind a Suprasil window. The output signals are digitized in a transient recorder with a minimum sample interval of 10 ns per 8-bit sample. Conversion of raw data into transient absorption vs. time and display of kinetically relevant functions are accomplished with a minicomputer. The experimental data are accumulated on magnetic tape and transferred to a large central computer facility where the final analysis of spectral and kinetic features takes place. Gas mixtures were prepared by admitting one component at a time and reading the corresponding partial pressure with a MKS Baratron Model 170 absolute electronic membrane manometer with a resolution of 10^{-5} bar.

Electric heating and temperature control provide a range of sample temperatures from 298 to 400 K. A platinum resistance thermometer is used to measure the temperature of the gas mixture near the central part of the irradiation cell traversed by the analyzing light beam. The temperature variation was ± 1 K.

Product Analysis. The products of radical combination and disproportionation reactions were analyzed by gas chromatography. Good separation of C_1 – C_4 hydrocarbons was obtained by using a $2\text{ m} \times \frac{1}{8}$ in. column with Poropak QS 60/80 mesh. After injection of the gas samples, the initial column temperature of 350 K was slowly increased to 450 K and the concentrations of the separated products were recorded with a flame ionization detector.

Computer Modeling. Computer simulation of chemical kinetics has become an important tool in studies of complex reaction mechanisms. We make use of a highly efficient computer program developed by Lang Rasmussen and Bjergbakke.¹⁴ As input the program accepts reaction schemes in the usual chemical notation. The program now translates the "chemical equations" into the pertinent set of differential equations which is solved by numerical integration after specification of initial concentrations, G values, and irradiation dose. A great advantage of this high-speed program is that the effect of parameter variation can be studied by

TABLE I: Composition of Gas Mixtures in Pulse Radiolysis Studies of Different C_2H_5 Source Reactions

reaction studied	chemical compositions	mole fraction	temp/K
S1	Ar/ $N_2(C_2H_5)_2$	1000:1	298
S2	Ar/CO(C_2H_5) ₂	1000:1	298
S3	Ar/ H_2O/C_2H_6	900:90:10	350
S4	H_2/C_2H_4	996:4	298

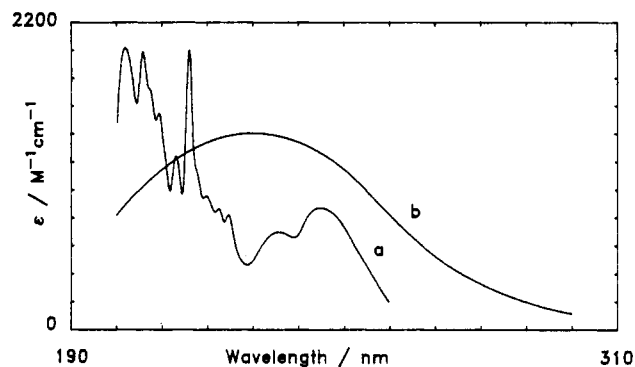


Figure 1. Absorption spectra of (a) ethyl radicals and (b) ethylperoxy radicals.

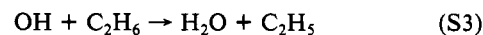
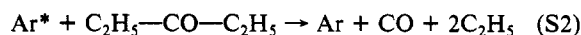
a semiinteractive procedure using a graphical computer terminal where calculated time profiles of selected species may be displayed together with stored experimental kinetic curves. The adjustment of model parameters to obtain a good fit with an experimental curve is achieved by a trial-and-error method which also provides a sensitivity test with respect to the variation of rate constants for each of the elementary reactions involved.

Since the experimental work has been carried out at fixed total pressure of $p(M) = p(H_2) = 1$ atm, we have applied equivalent second-order rate constants $k_{\text{eff}} = k(M)$ in the computer models to represent third-order reactions.

Materials. Ultrahigh-purity gases (ethane, ethylene, argon, and oxygen) were supplied from Matheson Gas Products. Diethyl ketone (p.a.) was used without further purification, and the water was triply distilled. Azoethane, containing less than 3% of impurities, was synthesized by O. Jørgensen at the Risø Chemistry Department. The liquid chemicals were thoroughly degassed on a high-vacuum line by trap-to-trap distillation before use.

Results and Discussion

Spectrum and Kinetics of C_2H_5 . In our attempts to obtain a clean source of ethyl radicals, we have compared the spectra of the transient species produced in the argon-sensitized radiolysis of azoethane and diethyl ketone, (S1) and (S2), and via the abstraction and addition reactions, (S3) and (S4). These source reactions were initiated by pulse radiolysis of the gas mixtures specified in Table I.



The transient absorption signals were measured with a band-pass of 4 Å which was chosen as the best compromise between spectral resolution and signal-to-noise ratio. The amount of stray light was measured by using suitable UV cutoff filters. Above 210 nm the measured stray light level was less than 2%. At 200 nm the stray light amounted to 5–10% depending on the optical alignment. Stray light corrections were applied to the transient absorption signals only in the 200–210-nm region.

The normalized absorption spectra, A/A_{max} , obtained with the four different gas mixtures were practically identical, i.e., within the experimental noise. Furthermore, the normalized absorption vs. time profiles, $A(t)/A_{\text{max}}$, monitored at different wavelengths were identical within each of the four series. These observations

(6) A. G. Gaydon, G. N. Spokes, and J. van Suchtelen, *Proc. R. Soc. London, A*, **256**, 323 (1960).

(7) D. A. Parkes and C. P. Quinn, *J. Chem. Soc., Faraday Trans. 1*, **72**, 1952 (1976).

(8) H. Adachi, N. Basco, and D. G. L. James, *Int. J. Chem. Kinet.*, **11**, 995 (1979).

(9) H. R. Wendt and H. E. Hunziker, *J. Chem. Phys.*, **81**, 717 (1984).

(10) H. Adachi, N. Basco, and D. G. L. James, *Int. J. Chem. Kinet.*, **11**, 1211 (1979).

(11) C. Anastasi, D. J. Waddington, and A. Woolley, *J. Chem. Soc., Faraday Trans. 1*, **79**, 505 (1983).

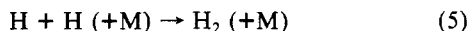
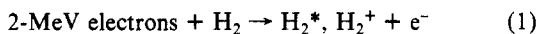
(12) P. B. Pagsberg, J. Eriksen, and H. C. Christensen, *J. Phys. Chem.*, **83**, 582 (1979).

(13) E. Bjarnov, J. Munk, O. J. Nielsen, P. Pagsberg, and A. Sillesen, *Risø-M-2366*, 1983.

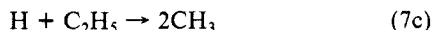
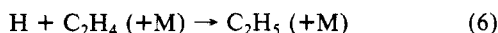
(14) O. Lang Rasmussen and E. Bjergbakke, *Risø-R-395*, 1984.

seem to indicate that the spectrum is due to light absorption by only one transient species, i.e., C_2H_5 formed via the source reactions (S1) through (S4).

As shown in Figure 1a, the spectrum of C_2H_5 is composed of two broad bands centered at 205 and 245 nm. The 205-nm band exhibits a partly resolved fine structure. Attempts to improve the spectral resolution were unsuccessful because of the decrease in the signal-to-noise ratio when the spectral band-pass was reduced. While there is no doubt that the two broad absorption bands must be assigned to the ethyl radical, it has not been possible to make a completely unambiguous assignment of the prominent 216-nm feature which coincides with the 3s Rydberg transition of the methyl radical. In the argon-sensitized reactions (S1) and (S2) it seems likely that, in addition to C_2H_5 , other fragments like CH_3 may be formed because $Ar(^3P_2)$ carries an excitation energy of 16 eV which is sufficient to break any of the molecular bonds. In the case of the simple abstraction reaction (S3) we observed that the rate of buildup of the absorbance monitored at 216 nm was equal to the decay rate of OH monitored at 309 nm. On the basis of the experimental decay curves, we calculated a value of $k(OH+C_2H_6) = (3.5 \pm 0.2) \times 10^8 M^{-1} s^{-1}$ at $T = 298 K$ which is in good agreement with previous studies.¹⁵ However, since equal amounts of H and OH are produced in the radiolysis of water vapor, we cannot rule out that part of the 216-nm absorbance may be due to methyl radicals formed via the consecutive reaction $H + C_2H_5 \rightarrow 2CH_3$. A major part of our experimental work has been devoted to studies of the yields and kinetics of C_2H_5 produced via (S4) initiated by pulse radiolysis of H_2/C_2H_4 mixtures. In this system H atoms are formed through the sequence (1)–(4)¹⁶ and recombining via (5):



The initial yield of H atoms was determined by addition of O_2 and monitoring the UV absorption of HO_2 formed via the reaction $H + O_2 + M \rightarrow HO_2 + M$. The HO_2 yield increased to a maximum at oxygen pressures above 10 mbar. From the maximum absorption we calculated $(H)_0 = A(210)_{\max}/(\epsilon x L) = (2.80 \pm 0.20) \times 10^{-7} M$ based on a recommended value of $\epsilon(210 \text{ nm}) = 1170 \pm 60 M^{-1}$ for the HO_2 radical.¹⁷ From the rate of formation monitored at 210 nm we have obtained a value of $k(H+O_2) = (4.5 \pm 0.5) \times 10^8 M^{-1} s^{-1}$ at $p(H_2) = 1 \text{ atm}$ and $T = 298 K$ in agreement with previous studies.¹⁸ In the pulse radiolysis of H_2/C_2H_4 mixtures ethyl radicals are formed and consumed via the reactions



The kinetics of C_2H_5 was studied over a wide range of ethylene concentrations by monitoring the transient absorption signals at 240 nm. The kinetic features were also monitored at 216 nm

(15) J. A. Kerr and S. J. Moss, Eds., *Handbook of Bimolecular and Termolecular Gas Reactions*, CRC Press, Boca Raton, FL, 1981.

(16) H. Eyring, J. O. Hirschfelder, and H. S. Taylor, *J. Chem. Phys.*, **4**, 479 (1936).

(17) T. T. Paukert and H. S. Johnston, *J. Chem. Phys.*, **56**, 2842 (1972).

(18) O. J. Nielsen, A. Sillesen, K. Luther, and J. Troe, *J. Phys. Chem.*, **86**, 2929 (1982).

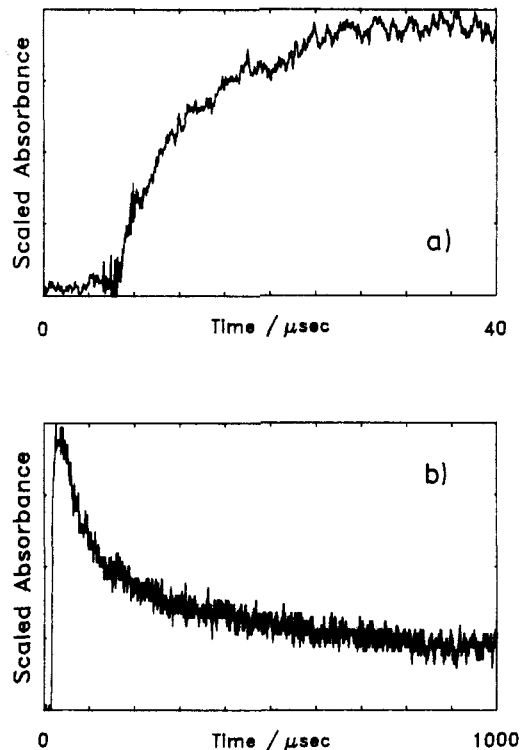


Figure 2. Typical formation (a) and decay curves (b) for ethyl radicals monitored at 240 nm.

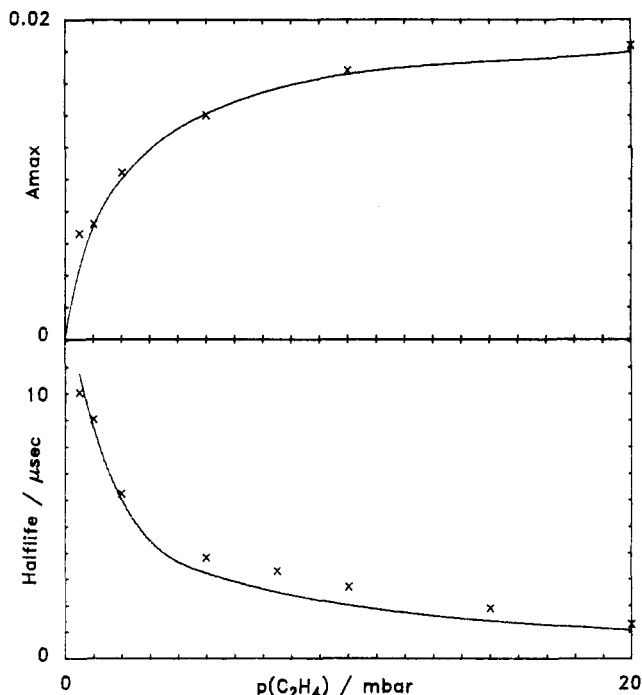


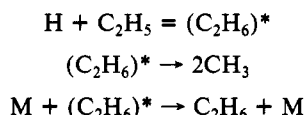
Figure 3. Experimental yields monitored at 240 nm (x) and model yields (smooth curve) of ethyl radicals along with observed (x) and model formation half-lives (smooth curve).

where CH_3 may contribute to the total absorbance. Typical formation and decay curves are shown in Figure 2 where the noise level corresponds to the employed spectral band-pass of 4 Å. At high ethylene concentrations practically all H atoms are converted into C_2H_5 and the kinetics is governed by reactions 6, 8a, and 8b. The experimental formation and decay half-lives measured at high ethylene concentrations were used to calculate approximate values of $k_6 = 6 \times 10^8 M^{-1} s^{-1}$ and $k_8 = 1.4 \times 10^{10} M^{-1} s^{-1}$ as well as the extinction coefficient $\epsilon(240) = 613 M^{-1} cm^{-1}$ by assuming that $(C_2H_5)_{\max} = (H)_0$. These trial values were adjusted in subsequent computer simulations of the complete model where the losses due to radical-radical reactions could be taken quantitatively into

TABLE II: Rate Constants at $p = 1$ atm and $T = 298$ K Obtained by Adjustment of Computer Model Kinetics to Experimental Results

reaction	$k/M^{-1} s^{-1}$	value derived from	observable
6	$(5.5 \pm 0.5) \times 10^8$	rate of C_2H_5 formation	$A(240)/\text{time}$
7a + 7b + 7c	$(1.7 \pm 0.2) \times 10^{11}$	yield of C_2H_5	$A(240)/p(C_2H_4)$
7a	$(9.0 \pm 1.0) \times 10^{10}$	yield of C_2H_6	GC analysis
7b	$(8.0 \pm 1.0) \times 10^{10}$	$k_7 - (k_{7c} + k_{7a})$	
7c	$(1.0 \pm 0.2) \times 10^{10}$	yield of $CH_3 + C_2H_5$	$A(216)/p(C_2H_4)$
8a + 8b	$(1.4 \pm 0.2) \times 10^{10}$	rate of C_2H_5 decay	$A(240)/\text{time}$
8a	$(1.0 \pm 0.2) \times 10^{10}$	yield of C_4H_{10}	GC analysis
8b	$(1.4 \pm 0.8) \times 10^9$	$k_{8b}/k_{8a} = 0.14$	GC analysis

account. The experimental yields of C_2H_5 are shown in Figure 3 along with the observed formation half-lives. The decrease in the yields at lower ethylene concentrations is primarily due to losses via reactions 7a–7c with a minor contribution from the slow recombination reaction (5). The variation in the formation half-lives deviates strongly from the simple hyperbolic expression $t_{1/2} = \ln 2/k_6(C_2H_4)_0$ which applies to reaction 6 in the absence of competing reactions. Thus, the short half-lives observed at the lower ethylene concentrations reflect an increase in the overall decay rate of H atoms due to reactions 7a–7c. The strategy employed in our computer simulations is outlined in Table II, which summarizes the stepwise evaluation of the rate constants for the individual elementary reactions. All computer simulations were carried out using the experimental value of $(H)_0 = 2.80 \times 10^{-7}$ M which forms the basis for the evaluation of the absolute bimolecular rate constants for the radical–radical reactions. At high ethylene concentrations the rates of formation and decay of C_2H_5 were governed solely by the values of k_6 and k_8 , and with the values quoted in Table II the model curves reproduced the experimental kinetics within the noise level exemplified in Figure 2. With fixed values of k_6 and k_8 the determination of k_7 was reduced to a one-parameter problem. As shown in Figure 3, the yields of C_2H_5 and the formation half-lives obtained with the model are in good agreement with the experimental values. The very high model value of $k_7 = 1.7 \times 10^{11} M^{-1} s^{-1}$ was necessary in order to reproduce the experimental results. This overall value corresponds to the sum of the rate constants for reactions 7a–7c. Reaction 7b, which is strongly exothermic, may be fast, and the combined effects of (6) and (7b) would be an increase in the rate of H atom recombination catalyzed by ethylene. Reactions 7a and 7c may be formulated as a two-channel chemical activation reaction:



The nascent $(C_2H_6)^*$ carries an excess energy $D(H-C_2H_5) = 98$ kcal/mol relative to the vibrational ground state of C_2H_6 . The excess energy must initially be localized in the H– C_2H_5 reaction coordinate which may be visualized as the $\nu_{10}(\text{Eg})$ normal mode of ethane. Energy randomization may take place through coupling between vibrational modes or by collisional relaxation. If the energy is shared equally by all of the 12 normal modes, the molecule will be in a state far below the threshold for dissociation into methyl radicals. Since $D(H_3C-CH_3) = 88$ kcal/mol, the dissociation requires a mechanism whereby about 90% of the available excess energy becomes localized in the C–C stretching mode, $\nu_3(A_{1g})$. Experimental evidence for reaction 7c has been obtained in experiments with a fast discharge flow reactor at low pressures^{19,20} where the collisional deactivation of $(C_2H_6)^*$ is too slow to prevent the rupture of the H_3C-CH_3 bond. Based on product analysis a value of $k_{7c} = 4.65 \times 10^{10} M^{-1} s^{-1}$ was obtained

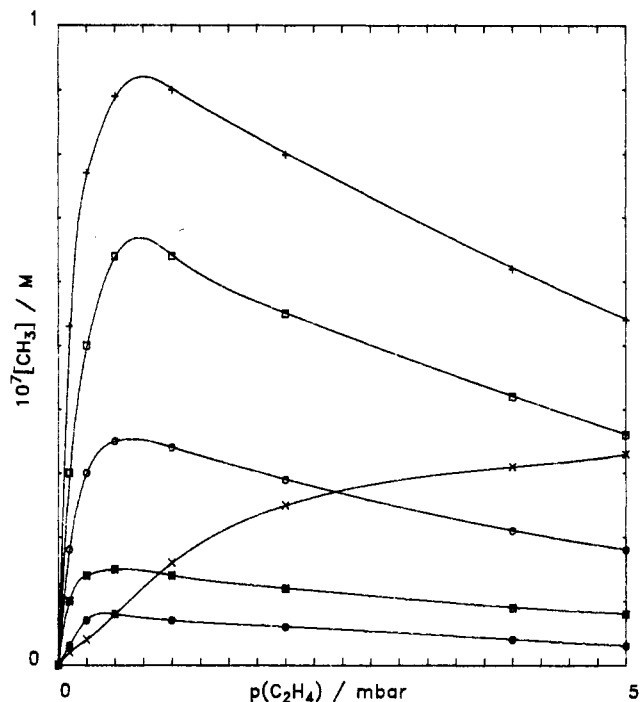


Figure 4. Yields of methyl radicals obtained by computer models with different values of k_{7c} keeping a constant value of $k_{7a} + k_{7c} = 1.7 \times 10^{11} M^{-1} s^{-1}$. The marks +, □, ○, and ■ correspond to $k_{7c} = 1.5 \times 10^{11}$, 1.0×10^{11} , 0.5×10^{11} , and $0.2 \times 10^{11} M^{-1} s^{-1}$, respectively. The curve marked × represents the experimental yields monitored at 216 nm, i.e., $A(216)/\epsilon L$ where $L = 120$ cm and $\epsilon = 10700 M^{-1} cm^{-1}$.

at 321 K and with a helium pressure of 8 Torr.²⁰ In the present spectrokinetic investigation a significant yield of CH_3 formed via (7c) should be directly observable by monitoring the transient absorption at 216 nm, which is indeed a prominent feature in the spectrum shown in Figure 1a. The proposed mechanism implies that the yield of methyl radicals goes through a maximum and subsequently decreases with increasing ethylene concentrations due to the competition between (6) and (7c). This general trend was verified by a series of computer simulations where the ratio k_{7c}/k_{7a} was varied while the sum was kept constant, $k_{7a} + k_{7c} = 1.7 \times 10^{11} M^{-1} s^{-1}$, $k_{7b} = 0$. The yields of methyl radicals obtained with the model are shown in Figure 4 along with experimental yields which were calculated by assuming that the total absorbance at 216 nm is due to CH_3 and using the most recent value of $\epsilon(CH_3) = 10700 M^{-1} cm^{-1}$.²¹ Clearly, the monotonic increase of $A(216)$ vs. $p(C_2H_4)$ is incompatible with reaction 7c which implies a maximum yield of CH_3 at $p(C_2H_4) = 0.8$ mbar. However, if methyl radicals produced via reaction 7c contribute to the transient absorption at 216 nm, we can estimate an upper limit of $k_{7c} = 10^{10} M^{-1} s^{-1}$.

Thus, at $p(H_2) = 1$ atm it appears that reaction 7c plays a minor role compared with the competing reactions (7a) + (7b) proceeding with an overall rate constant of $k_{7a} + k_{7b} = k_7 - k_{7c} = 1.6 \times 10^{11} M^{-1} s^{-1}$. The ratio of k_{7a}/k_{7b} was determined by GC analysis of the stable products formed by pulse radiolysis of H_2 containing 0.4% C_2H_4 where the relative yield of C_2H_5 is about 60% as shown in Figure 2. The main products were C_4H_{10} and C_2H_6 , and assuming that the only source reactions are (8a), (8b), and (7a), the corresponding rate constants listed in Table II were determined by adjusting the model to reproduce the experimental yields. The kinetic results are in close agreement with existing data.¹⁵ The fraction of the C_2H_6 yield originating from (8b) was accounted for by using a consensus value of $k_{8b}/k_{8a} = 0.14$.¹⁵ An experimental yield of 15% C_3H_8 was taken as strong evidence for the presence of CH_3 , and with an estimated C_2H_5/CH_3 ratio of 10:1 a major fraction of the methyl radicals is expected to react via $CH_3 + C_2H_5 \rightarrow C_3H_8$. However, methyl radicals originating

(19) P. Camilleri, R. M. Marshall, and J. H. Purnell, *J. Chem. Soc., Faraday Trans. 1*, **70**, 1434 (1974).

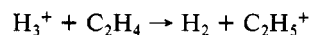
(20) G. Pratt and I. Veltman, *J. Chem. Soc., Faraday Trans. 1*, **72**, 1733 (1976).

(21) M. T. Macpherson, M. J. Pilling, and M. J. C. Smith, *J. Phys. Chem.*, **89**, 2268 (1985).

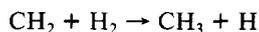
TABLE III: Rate Constants of the Reaction $C_2H_5 + O_2 + M \rightarrow C_2H_5O_2 + M$ Monitored at 240 nm and at $p(H_2) = 1$ atm

$10^{-9}k/M^{-1} s^{-1}$	temp/K				
	298	325	346	376	400
	3.2 ± 0.1	3.0 ± 0.2	2.7 ± 0.1	2.5 ± 0.1	2.2 ± 0.2

from reaction 7c cannot account for the experimental results, and we have considered other possible source reactions for CH_3 . The reactions which may be important only at higher ethylene concentrations are proton transfer followed by neutralization, in competition with reaction 4



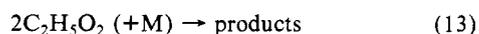
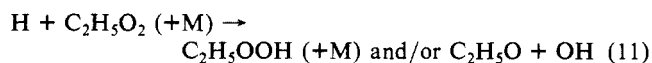
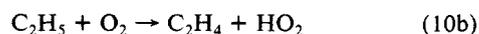
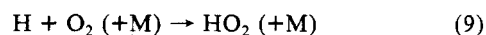
Methylene formed in the reaction above or by direct excitation of ethylene, $(C_2H_4)^* \rightarrow 2CH_2$, may be converted into CH_3 via



However, the experimental data base which is available at present did not allow us to distinguish between alternative CH_3 sources. All we can say with some degree of confidence is that the chemical activation channel (7c) appears to be unimportant at $p(H_2) = 1$ atm.

Judging from the close similarities in the yields and the rates of formation and decay monitored at 216 and 240 nm, it appeared as if only one species was present, i.e., C_2H_5 . It seems most likely though that the experimental yield of propane originates from the combination of CH_3 with C_2H_5 . The experimental yield of 15% C_3H_8 is compatible with the maximum yield of CH_3 calculated by assuming that the total absorbance at 216 nm is due to CH_3 . The lack of a detailed mechanism for the formation and decay of CH_3 calls for an estimate of the uncertainty in the rate constants evaluated with a computer model neglecting the presence of CH_3 . The error limits estimated in Table II are based on a sensitivity analysis of the curve-fitting procedures taking into account the signal-to-noise ratio of the experimental kinetic curves as well as uncertainties in the reading of the partial pressure of C_2H_4 . The values of extinction coefficients shown in Figure 1 were derived from the maximum of transient absorption signals, $A_{max} = \epsilon L - (C_2H_5)_{max}$, and relative yield of ethyl radicals, $(C_2H_5) = f(H)_0$. The value of $(H)_0 = (2.8 \pm 0.20) \times 10^{-7}$ M was calculated from the yield of HO_2 obtained at high oxygen concentration and by using a consensus value of $\epsilon(HO_2)_{210} = (1170 \pm 60) M^{-1} m^{-1}$.¹⁷ The fractional yield, f , was determined by computer modeling of A_{max} vs. $p(C_2H_4)$ taking into account the complete mechanisms, i.e., reactions 5 through 8. A conservative estimate of uncertainty in the values of extinction coefficients in Figure 1 amounts to $\pm 15\%$. Thus, the extinction coefficients at the two maxima are $\epsilon_{205} = 2010 \pm 300 M^{-1} cm^{-1}$ and $\epsilon_{245} = 870 \pm 130 M^{-1} cm^{-1}$.

Spectrum and Kinetics of $C_2H_5O_2$. When small amounts of oxygen are added to C_2H_4/H_2 mixtures, the spectrum of C_2H_5 observed at short delay times is gradually replaced by a different spectrum, which we assign to the radical adduct $C_2H_5O_2$. The spectrum in Figure 1b shows the maximum absorbance occurring about 40 μs after pulse irradiation of a gas mixture composed of 1 mbar of O_2 plus 5 mbar of C_2H_4 in 1 atm of H_2 . In the presence of oxygen the following reactions have been taken into account:



The continuous spectrum in Figure 1b is clearly different from the structured spectrum of C_2H_5 . The spectrum is also different

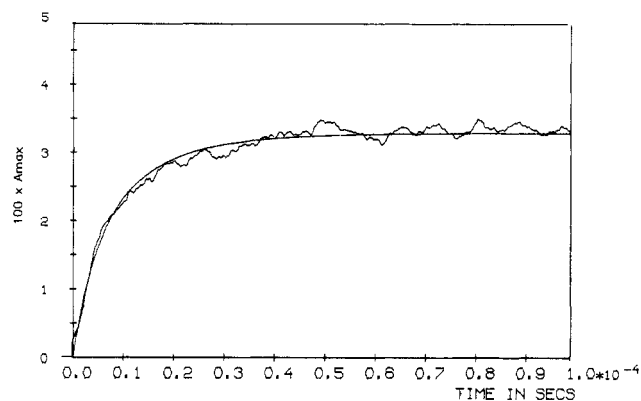


Figure 5. Formation kinetics of ethylperoxy radicals. Transient absorption signal monitored at 240 nm (noisy curve) and simulated compound absorbance, $A(C_2H_5) + A(C_2H_5O_2)$ (smooth curve).

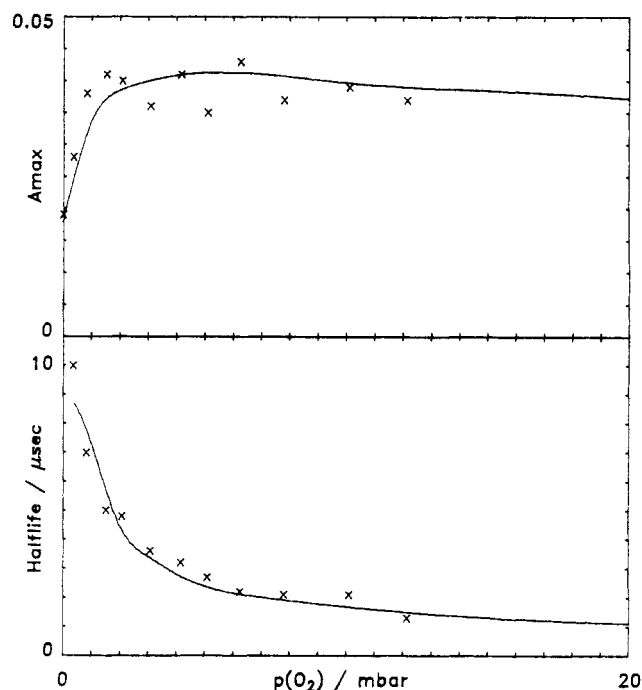


Figure 6. Experimental yields monitored at 240 nm (x) and model yields (smooth curve) of ethylperoxy radicals along with observed (x) and model formation half-lives (smooth curve).

from the well-known spectrum of HO_2 which has an absorption maximum at about 205 nm.¹⁷ The spectral assignment is supported by our kinetic observations. Figure 5 shows the kinetics of $C_2H_5O_2$ formation monitored at 240 nm. The fast initial absorption buildup is due to C_2H_5 formed via reaction 6 while the subsequent slower formation corresponds to the replacement by the more strongly absorbing $C_2H_5O_2$ radical via (10a). We chose 240 nm as the most suitable wavelength for the kinetic studies because the possible interference from HO_2 , which may originate from several source reactions, would be negligible at this wavelength. The yield of $C_2H_5O_2$ and the rate of its formation were studied with constant values of $p(H_2) = 990$ mbar and $p(C_2H_4) = 20$ mbar and by varying $p(O_2)$ from 0.2 to 6.0 mbar. At the lower oxygen concentrations the loss of H atoms in reaction 9 is unimportant in comparison with reaction 6. However, at the higher oxygen concentrations reaction 9 becomes increasingly important as shown in Figure 6. Model calculations with $\epsilon - (C_2H_5O_2)$ and the rate constants for reactions 10–13 as adjustable

parameters were compared with the experimental results. The smooth curve included in Figure 5 shows the calculated time profile of the compound absorption, $A(\text{C}_2\text{H}_5) + A(\text{C}_2\text{H}_5\text{O}_2)$, obtained with the values $\epsilon(\text{C}_2\text{H}_5) = 670 \text{ M}^{-1} \text{ cm}^{-1}$ and $\epsilon(\text{C}_2\text{H}_5\text{O}_2) = 1360 \text{ M}^{-1} \text{ cm}^{-1}$ and the rate constant $k_{10a} = 3.2 \times 10^9 \text{ M}^{-1} \text{ s}^{-1}$. The close agreement between the model and the experimental results supports the spectral assignments as well as the kinetic results.

The calculated yield of $\text{C}_2\text{H}_5\text{O}_2$ at low oxygen pressures was found to be very sensitive to the value of k_{12} . With a value of $k_{12} = 6.0 \times 10^{10} \text{ M}^{-1} \text{ s}^{-1}$ we obtained a good fit to the experimental yields and formation half-lives as shown in Figure 6. The decay of $\text{C}_2\text{H}_5\text{O}_2$ followed simple second-order kinetics, and the calculated rate constant $k_{13} = 3.15 \times 10^7 \text{ M}^{-1} \text{ s}^{-1}$ in fair agreement with the results of previous studies, $(6.0 \pm 0.6) \times 10^7 \text{ M}^{-1} \text{ s}^{-1}$ and $(3.5 \pm 0.3) \times 10^7 \text{ M}^{-1} \text{ s}^{-1}$.¹¹ Using the same procedures, we studied the addition reaction (10a) in the range of 298–400 K, and the results are collated in Table III. When presented in terms of an Arrhenius equation, the results show an apparent small negative activation energy, $\log k_{10a}/\text{M}^{-1} \text{ s}^{-1} = (8.90 \pm 0.04) + (840 \pm 70 \text{ cal mol}^{-1})/2.303RT$, where the error limits represent the standard deviations. Prior to this study, there were no direct measurements of the rate constant k_{10a} . Early, indirect estimates of the rate constant k_{10a} , derived from complex reaction systems, lie in the range from $6 \times 10^7 \text{ M}^{-1} \text{ s}^{-1}$ at 308 K and 47 mbar²² to $1.2 \times 10^9 \text{ M}^{-1} \text{ s}^{-1}$ at 348–575 K and 6 mbar²³ and $4.2 \times 10^9 \text{ M}^{-1} \text{ s}^{-1}$ at 295 K and pressures of 6–137 mbar.²⁴ Recently, very

extensive studies of the overall rate constant $k_{10} = k_{10a} + k_{10b}$ for the $\text{C}_2\text{H}_5 + \text{O}_2$ reactions and their branching fractions have been performed by Slagle and Gutman²⁵ and by Plumb and Ryan.²⁶ In their studies the C_2H_5 radical decay was monitored directly by photoionization mass spectrometry, and special attention was given to obtain the pressure dependence in the falloff region, 0.5–10 mbar, of k_{10} ²⁵ and k_{10a} .²⁶ If we take into account that at room temperature the fraction of reaction 10 producing C_2H_4 and HO_2 is small (ca. 5%)^{24,26} and that this reaction is independent of the pressure,²⁶ then our value of k_{10a} at room temperature may be taken as the high-pressure limit of $k_{10} = k_{10a}$. The value of $k_{10a} = 3.2 \times 10^9 \text{ M}^{-1} \text{ s}^{-1}$ obtained in this study at 298 K and 1 atm of H_2 is in agreement with that of $2.7 \times 10^9 \text{ M}^{-1} \text{ s}^{-1}$ at 295 K and 1 atm of He predicted by Plumb and Ryan²⁶ on the basis of their experimental data at low pressures and Troe's theory.²⁷

Acknowledgment. We thank H. Egsgaard for carrying out the GC analysis and P. L. Genske for his technical assistance. We are also grateful to D. Gutman and I. R. Slagle for providing a preprint of their work. Finally, we acknowledge many valuable discussions with our highly esteemed colleague, the late Gösta Nilsson.

Registry No. H, 12385-13-6; H_2 , 1333-74-0; C_2H_4 , 74-85-1; O_2 , 7782-44-7; C_2H_5 , 2025-56-1; $\text{C}_2\text{H}_5\text{O}_2$, 3170-61-4.

(22) J. E. Jolly, *J. Am. Chem. Soc.*, **79**, 1537 (1957).

(23) I. I. Avremenko and R. V. Kolesnikova, *Izv. Akad. Nauk SSSR, Otd. Khim. Nauk*, 806, 989 (1960).

(24) D. P. Dingley and J. G. Calvert, *J. Am. Chem. Soc.*, **85**, 856 (1963).

(25) I. R. Slagle, Q. Feng, and D. Gutman, *J. Phys. Chem.*, **88**, 3648 (1984).

(26) I. C. Plumb and K. A. Ryan, *Int. J. Chem. Kinet.*, **13**, 1011 (1981).

(27) J. Troe, *J. Phys. Chem.*, **83**, 114 (1979).

Intercalation Kinetics of Alkali-Metal Ions Into γ -Zirconium Phosphate Using the Pressure-Jump Technique

Naoki Mikami, Minoru Sasaki, Naofumi Kawamura, Kim F. Hayes,¹ and Tatsuya Yasunaga*

Department of Chemistry, Faculty of Science, Hiroshima University, Hiroshima 730, Japan
(Received: March 26, 1985)

The intercalation kinetics of a series of alkali-metal ions, Li^+ , Na^+ , K^+ , Rb^+ , and Cs^+ , into γ -zirconium phosphate (γ -ZrP) were studied by using the pressure-jump technique with conductivity detection. In aqueous suspensions of γ -ZrP containing alkali-metal ions, double relaxations of the order of milliseconds were observed under the experimental condition that the amount of alkali-metal ion adsorbed is more than half of the ion-exchange capacity of γ -ZrP, $3.12 \times 10^{-3} \text{ mol dm}^{-1}$. Both fast and slow relaxation times increase with the concentration of alkali-metal ion. From the kinetic and static results obtained, the fast and slow relaxations were attributed to the entering and interlayer diffusion processes of alkali-metal ions in γ -ZrP, respectively. The forward rate constants for these processes are closely related to the interlayer distance of alkali-metal intercalation compounds of γ -ZrP and are smaller than those reported in the α -ZrP-alkali-metal ions system. The difference between the rate constants for α - and γ -ZrP could be interpreted by the difference between the acidities of the phosphate groups in α - and γ -ZrP.

Introduction

Zirconium phosphate, $\text{Zr}(\text{HPO}_4)_2 \cdot n\text{H}_2\text{O}$, has several layered crystalline structures such as $\text{Zr}(\text{HPO}_4)_2 \cdot \text{H}_2\text{O}$ (α -ZrP) and $\text{Zr}(\text{HPO}_4)_2 \cdot 2\text{H}_2\text{O}$ (γ -ZrP) and forms various intercalation compounds as a result of intercalation of guest donors into its interlayers.²⁻⁷ In particular, γ -ZrP has interesting characteristics

compared with α -ZrP; the γ -form of the crystal not only has a relatively long interlayer distance of 12.3 Å but also a densely linked layered structure, and the phosphate groups in the compound exhibits strong acidity.^{8,9} The study of intercalation dy-

(1) Japanese Ministry of Education Research Scholar. Permanent address: Environmental Engineering and Science, Department of Civil Engineering, Stanford University, Stanford, CA 94305.

(2) Clearfield, A.; Blessing, R. H.; Stynes, J. A. *J. Inorg. Nucl. Chem.* **1968**, *30*, 2249.

(3) Clearfield, A.; Smith, G. D. *Inorg. Chem.* **1969**, *8*, 431.

(4) Clearfield, A.; Duax, W. L.; Medina, A. S.; Smith, G. D.; Thomas, J. R. *J. Phys. Chem.* **1969**, *73*, 3424.

(5) Clearfield, A.; Garces, J. M. *J. Inorg. Nucl. Chem.* **1979**, *41*, 879.

(6) Alberti, G. *Acc. Chem. Res.* **1978**, *11*, 163.

(7) Alberty, G.; Costantino, U. *Intercalation Chemistry*; Whittingham, M. S., Jacobson, A. J., Eds.; Academic Press: New York, 1982; Chapter 5, p 147.

(8) Yamanaka, S.; Tanaka, M. *J. Inorg. Nucl. Chem.* **1979**, *41*, 45.

(9) Sasaki, M.; Mikami, N.; Ikeda, T.; Hachiya, K.; Yasunaga, T. *J. Phys. Chem.* **1982**, *86*, 5230.